

# Effect of water intercalation on $\text{VO}_x$ layers in dodecylamine-intercalated vanadium oxide nanotubes

Hyocheon Kweon, Kyu Won Lee, Eun Mo Lee, Jitae Park, I-M. Kim, and Cheol Eui Lee\*

*Department of Physics and Institute for Nano Science, Korea University, Seoul 136-713, Korea*

G. Jung

*Department of Physics, BGU of the Negev, PO Box 653, Beer-Sheva 84105, Israel*

A. Gedanken and Yu. Koltypin

*Department of Chemistry, Bar-Ilan University, Ramat-Gan 52900, Israel*

(Received 13 December 2006; revised manuscript received 17 May 2007; published 31 July 2007)

Dodecylamine-intercalated vanadium oxide nanotubes were obtained by distinct synthesis processes. Water intercalation in the nanotube structure was identified in a marked manner by the distortion of the  $\text{VO}_x$  layers in the x-ray diffraction patterns and enhanced  $\text{V}^{4+}=\text{O}$  absorption in the Fourier-transform infrared spectra. Our electron spin resonance measurements sensitively reflect changes in the microscopic structure and magnetic interactions introduced by the water intercalation in the vanadium oxide nanotubes.

DOI: [10.1103/PhysRevB.76.045434](https://doi.org/10.1103/PhysRevB.76.045434)

PACS number(s): 81.07.De, 76.30.-v

## I. INTRODUCTION

Quasi-one-dimensional nanostructures are attracting considerable interest, especially for technological applications such as catalysts, sensors, and electrodes.<sup>1-5</sup> Of particular interest are the vanadium oxide nanotubes ( $\text{VO}_x$ -NTs). Vanadium oxides ( $\text{VO}_x$  with  $1.0 < x < 2.5$ ), with mixed valency typically of  $\text{V}^{4+}$  and  $\text{V}^{5+}$ , constitute a class of compounds widely used as cathode materials in the Li-ion batteries.<sup>3,4,6-9</sup> The electrical conduction mechanism of  $\text{VO}_x$  is generally taken to be electron hopping between  $\text{V}^{5+}$  and  $\text{V}^{4+}$ .<sup>4</sup> They can undergo a metal-to-Mott insulator transition, become superconductive, or show unusual quantum spin states.<sup>10,11</sup> The  $\text{VO}_x$ -NTs were observed to be a frustrated spin liquid, in which the electron spins have random orientations, with approximately one spin for each of the three V sites.<sup>6</sup> The octahedral V(1) and V(2) sites constitute a double layer, the tetrahedral V(3) site lying between them.<sup>12</sup> The spins in the octahedral sites (chain sites) are strongly antiferromagnetically correlated, some of them being coupled in dimers exhibiting a spin-gap behavior and the others forming trimers. Due to the spin frustration, the tetrahedral magnetic sites are only weakly correlated.<sup>12</sup> The V(3) site lying in the deepest energy level of vanadium sites is also the most deeply buried in the structure, and the V(1) site lying in the highest level is also the most exposed one, indicating that V(1) is the doping-sensitive site.<sup>6</sup> The electrical and magnetic properties of  $\text{VO}_x$ -NTs may be controlled by electron or hole doping.<sup>6,13</sup>

In this work, we address the effects of the intercalated water molecules in  $\text{VO}_x$ -NTs, giving rise to a change in the layered structure and physical properties.  $\text{V}_2\text{O}_5$  xerogel ( $\text{V}_2\text{O}_5 \cdot n\text{H}_2\text{O}$ ) has been obtained either by protonation of vanadates in aqueous solutions or by hydrolysis and condensation of  $\text{V}_2\text{O}_5$ .<sup>1,2,14</sup> Water molecules intercalated in the  $\text{VO}_x$  layered structure may be introduced during the synthesis by cation-exchange, acid-base chemistry, or redox reactions and may give rise to amorphization of the  $\text{VO}_x$  layered structure.<sup>4,15-18</sup> In order to obtain a deeper insight into the

$\text{VO}_x$ -NTs, we have carried out x-ray diffraction (XRD), Fourier-transform infrared (FTIR) spectroscopy, as well as electron spin resonance (ESR) measurements. In particular, ESR was employed to obtain information on the water intercalation effect on the  $\text{V}^{4+}$  ions, which are responsible for the electrical and magnetic properties of the nanotubes.

## II. EXPERIMENT

Two distinct synthesis processes with same starting materials were followed in this work. In the “powder” method,<sup>7</sup>  $\text{V}_2\text{O}_5$  powder (Sigma) and dodecylamine (Aldrich, 98%) in a molar ratio of 2:1 were added to ethanol and stirred for 2 h in air. The resulting yellow solution adduct was reacted with de-ionized water and stirred for 48 h at room temperature. In the “sol-gel” method,<sup>14</sup>  $\text{V}_2\text{O}_5 \cdot n\text{H}_2\text{O}$  gels were obtained from  $\text{V}_2\text{O}_5$  (Aldrich) dissolved in a solution of hydrogen peroxide (Aldrich, 30%) and stirred for 24 h at room temperature. The gels were then added to dodecylamine (Aldrich, 98%) in a molar ratio of 2:1 and stirred for 24 h. After each process, the composites were transferred to an autoclave at 180 °C for ten days and washed with ethanol and de-ionized water. The resultant solids were dried at 80 °C for 6 h in air. The samples obtained through the sol-gel method (“SVNT”) and the powder method (“PNVT”) were used for this work. The FTIR spectra were taken using a Bomem MB spectrometer, with a slit resolution of 0.2 nm, and a JEOL JES-FA200 spectrometer was used for the ESR experiment at 9 GHz.

## III. RESULTS AND DISCUSSION

Figure 1 shows the XRD patterns for PVNT and SVNT, both displaying low-angle reflection peaks characteristic of the layered structure. The interlayer distances were measured to be 3.04 nm (SVNT) and 2.78 nm (PVNT), comparable to previous reports (2.74 nm).<sup>3</sup> The greater interlayer distance of SVNT is indicative of water molecules intercalated between the  $\text{VO}_x$  layers in addition to dodecylamine,<sup>14</sup> in contrast to the case of PVNT. The high-angle reflection peaks of

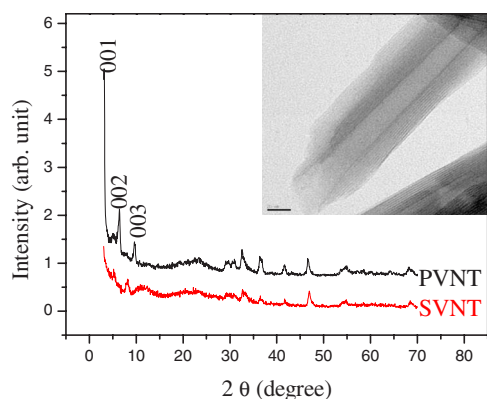


FIG. 1. (Color online) X-ray powder diffraction patterns of the  $\text{VO}_x$ -NTs obtained through distinct routes. Inset: transmission electron microscope (TEM) image of the PVNT.

the  $\text{VO}_x$ -NTs are dissonant, indicating that the  $\text{VO}_x$  layers in the SVNT are slightly distorted due to the intercalated water molecules.<sup>7</sup> The transmission electron microscope (TEM) image (inset of Fig. 1) shows the PVNT multiwall nanotubes with a quasilayered structure, consisting of concentric shells, with an average outer diameter of 70.48 nm and interlayer distance of 2.67 nm.<sup>3,8,13</sup>

Figure 2 shows the FTIR spectra of the  $\text{VO}_x$ -NTs. The peaks in the 500–1000  $\text{cm}^{-1}$  range can be attributed to various vibrations of the V—O type.<sup>19</sup> In particular, the peaks at 1013 and 997  $\text{cm}^{-1}$  can be assigned to the  $\text{V}^{5+}=\text{O}$  stretching mode, and those at 999 and 971  $\text{cm}^{-1}$  can be attributed to the  $\text{V}^{4+}=\text{O}$  bonds.<sup>20</sup> As shown in the inset of Fig. 2, the absorption peak corresponding to the  $\text{V}^{4+}=\text{O}$  bonds in the SVNT is stronger than that in the PVNT, which indicates that water intercalation gives rise to an increase in the  $\text{V}^{4+}$  concentration. The two peaks manifested in the 2800–3000  $\text{cm}^{-1}$  frequency range reflect the C—H stretching mode.<sup>8,9,13,19,21</sup> The bending vibrations of the H—O—H (around 1600  $\text{cm}^{-1}$ ) and V—O—V (around 500  $\text{cm}^{-1}$ ) bonds are also apparent.<sup>19</sup> The absorption intensity of the H—O—H stretching in the SVNT is much stronger than that in the PVNT, indicative of the water intercalation in the

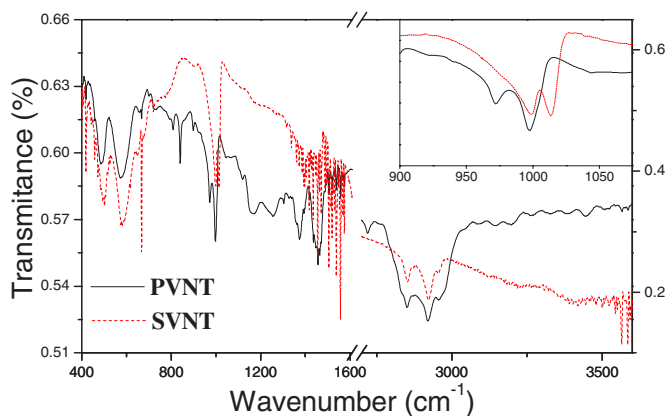


FIG. 2. (Color online) FTIR spectra of the PVNT and the SVNT. Inset: the absorption peaks corresponding to the  $\text{V}^{5+}=\text{O}$  and the  $\text{V}^{4+}=\text{O}$  bonds. An increase in the  $\text{V}^{4+}=\text{O}$  absorption peak in the SVNT is noticed.

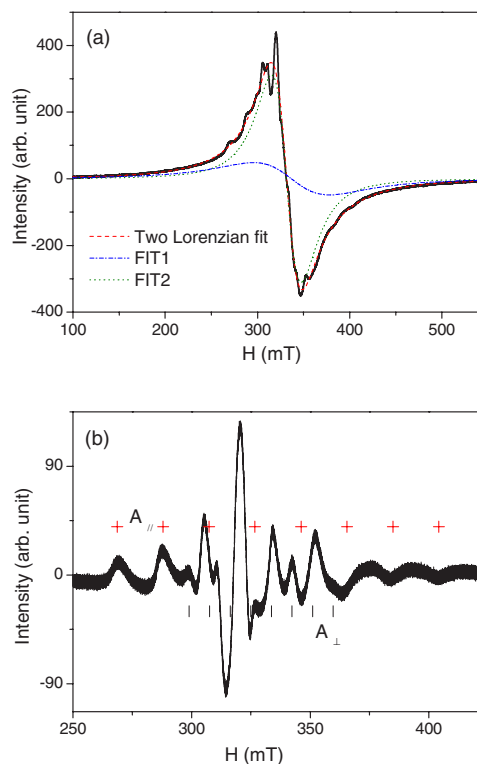


FIG. 3. (Color online) (a) SVNT ESR spectrum at 400 K fitted by two Lorentzian line components and (b) the residual hyperfine structure obtained by subtraction of the Lorentzian fits.

SVNT. In the  $\text{VO}_x$ -NTs, evidence for the protonation of alkyamine ( $\text{NH}_2 \rightarrow \text{NH}_3^+$ ) has been seen by the absorptions assigned to a  $\text{NH}_3^+$  vibration (3500–3300  $\text{cm}^{-1}$ ).<sup>20,21</sup> The protonation by intercalated water molecules gives rise to a distortion of the  $\text{VO}_x$  layer,<sup>4</sup> as seen in the V—O—V equatorial stretching. The redshifts, of the 595.2  $\text{cm}^{-1}$  peak to 561.3  $\text{cm}^{-1}$  and of the 502.2  $\text{cm}^{-1}$  peak to 477.0  $\text{cm}^{-1}$ , with increasing sheet distance are associated with the stretching vibration modes of the O— $\text{V}_3$  and O— $\text{V}_2$  bonds in a disordered V—O—V framework.<sup>8,19–21</sup>

Figure 3 shows an ESR line shape in SVNT fitted by two Lorentzian line components (FIT1 and FIT2) and the residual hyperfine spectrum obtained by subtraction of the Lorentzian fits.<sup>22,23</sup> The ESR intensity arising from the  $\text{V}^{4+}$  concentration is stronger in SVNT than that in PVNT, indicating that the water intercalation gives rise to the electron transfers. The hyperfine-split line arising from the isolated spins is also much stronger in the SVNT than in the PVNT, with its areal fraction being about 1%. The eight-line hyperfine splitting structure indicates that the 3d electrons of the  $\text{V}^{4+}$  ion are strongly localized, interacting with only one vanadium nucleus.<sup>24</sup> The ESR line shape of the two Lorentzian line components superposed by a hyperfine structure indicates that the  $\text{V}^{4+}$  ions are inhomogeneously distributed. The intercalated water molecules would act to increase the inhomogeneity in the vanadium oxide nanotubes. Considering that the V(1) site is the doping-sensitive one, the hyperfine-split lines may be ascribed to the isolated  $\text{V}^{4+}(1)$  ions.<sup>25</sup>

In a powder, the hyperfine spectrum of the superposition of all the orientations is very complicated and poorly re-

TABLE I. Principal values of the hyperfine structure at 400 K. The principal  $z$  axis corresponds to the direction normal to the vanadium oxide layer. The values for a V<sub>2</sub>O<sub>5</sub> single crystal were cited from Ref. 22.

	$g_{\perp}$	$g_{\parallel}$	$g_{aver}$	$A_{\perp}$ (mT)	$A_{\parallel}$ (mT)
V <sub>2</sub> O <sub>5</sub>	1.98	1.92	1.96	6.6	18.4
SVNT	1.96	1.92	1.95	8.7	19.3
PVNT	1.98	1.92	1.96	7.8	18.4

solved. As was reported in a previous ESR study of amorphous V<sub>2</sub>O<sub>5</sub>, the large anisotropy of hyperfine coupling may give a much simpler spectrum.<sup>24</sup> ESR spectra of V<sub>2</sub>O<sub>5</sub> single crystal have usually been described by a uniaxial  $g$  tensor and a hyperfine coupling tensor, with their principal  $z$  axis corresponding to the direction normal to the vanadium oxide layer. The uniaxial  $g$  tensor and the hyperfine coupling tensor were obtained from the ESR spectra, as shown in Table I.<sup>22-24</sup> The  $g$  tensor was determined by the center fields of the hyperfine spectra. Due to the weak hyperfine spectrum, the parameters of the PVNT include larger uncertainties than those of SVNT and the parameters perpendicular to the  $z$  axis are more erroneous than those parallel to the  $z$  axis. The greater hyperfine splitting in SVNT indicates the stronger hyperfine interaction and thus the stronger localization of the  $3d$  electrons at the V<sup>4+</sup>(3) site in SVNT. This may be ascribed to the intercalated water molecules accompanying a structural change, as seen by the redshifts in the V—O—V stretching modes in the FTIR spectra (Fig. 2).<sup>4,15</sup>

The spin susceptibilities, in Fig. 4, were obtained from the ESR intensity for the two Lorentzian line components, FIT1 and FIT2 lines. The susceptibility of the FIT1 line component in PVNT in Fig. 4(a) is shown to be much greater than that of the FIT2 line component. According to previous reports,<sup>6,12</sup> there are three types of spin complexes in the system: quasifree spins at the V(3) sites and spin dimers and trimers comprising the V(1) and V(2) sites. Thus, the FIT2 line component of PVNT, without water intercalation, exhibiting only a simple paramagnetic behavior at all temperatures, can readily be ascribed to the quasifree spins at the V(3) site, which is known to be nearly decoupled from the V(1) and V(2) sites due to the frustration of the exchange coupling. On the other hand, the FIT1 line of PVNT can be assigned to the V(1) and V(2) sites, for which the spin susceptibility is dominated by the spin trimers in the low temperature region and by the spin dimers in the high temperature region because of the spin gap and singlet-triplet excitation of spin dimers.<sup>12</sup> Owing to thermally activated singlet-triplet excitation across the dimer gap, the ESR susceptibility of the antiferromagnetic spin dimers in PVNT can be observed to increase with increasing temperature in the high temperature region.

As shown in Fig. 4(b), while the total ESR spin susceptibility for SVNT is apparently much greater than that for PVNT in agreement with the increase in the IR absorption peak of the V<sup>4+</sup>=O bond, the ESR susceptibility of the FIT1 line in SVNT is comparable to that of the FIT2 line.

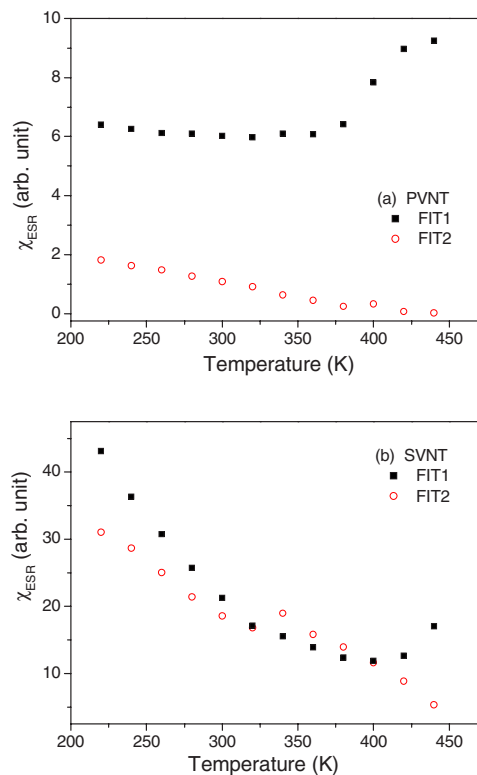


FIG. 4. (Color online) Spin susceptibilities for the ESR line components of (a) PVNT and (b) SVNT as a function of temperature.

This indicates that the fitted ESR lines have distinct origins in PVNT and SVNT, calling for distinct line assignments. In fact, according to the literature, while the V(3) site is considered to be doping insensitive, electron doping to the V(1) site, presumably taking place by water intercalation in our case, is known to remove the spin frustration between the V(2) and V(3) sites.<sup>6</sup> Once the spin frustration is removed, a strong exchange interaction between the V(2) and V(3) sites renders the two sites indistinguishable in ESR. The interacting V(2)-V(3) sites are decoupled from the spin dimers and trimers, as there are no unpaired spins on the nearby V(1) sites. Therefore, the interacting V(2)-V(3) sites as well as the quasifree V(3) site can be assigned to the FIT2 line in SVNT, the intensity of which becomes much larger than that of the FIT2 line in PVNT. Thus, the relative increase in the FIT2 line intensity and the relative decrease in the FIT1 line intensity in SVNT can be systematically explained by assuming electron doping effect arising from the water intercalation. Nonetheless, the spin susceptibility of the FIT1 line in SVNT still appears to be dominated by the spin trimers in the low temperature region and by the spin dimers in the high temperature region as in the case of PVNT.

Figure 5 shows the ESR linewidth of the FIT1 line in the two VO<sub>x</sub>-NTs as a function of temperature. In both VO<sub>x</sub>-NTs, it increases with increasing temperature, whereas the ESR linewidths for the other ESR lines show little temperature dependence, with the ESR linewidth of FIT2 line being about 53.1 mT and the hyperfine structure linewidth being about 19.4 mT in SVNT, and the ESR linewidth of FIT2 line being about 17.5 mT in PVNT. The hyperfine

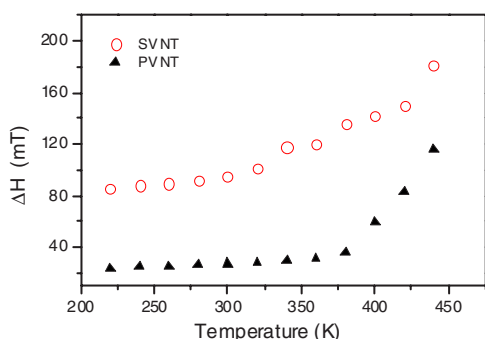


FIG. 5. (Color online) ESR linewidths of the FIT1 line in the  $\text{VO}_x$ -NTs as a function of temperature.

structure linewidth in SVNT is greater than the linewidth of FIT2 line in PVNT. Since the hyperfine structure originates from the isolated spins, the line broadening of the hyperfine structure may be ascribed to the structural distortion of the  $\text{VO}_x$  layers, giving rise to a change in the hyperfine splitting. The larger FIT2 linewidth in SVNT than in PVNT may be attributed to the antiferromagnetic correlation between the V(2) and V(3) sites; the FIT2 line in PVNT arises from quasifree spins on the V(3) site, whereas the FIT2 line in SVNT includes a large contribution from the antiferromagnetically correlated V(2) and V(3) sites as well as the quasifree spins. The increase in the FIT1 linewidth with increasing temperature can be attributed to mobile holes, giving rise to spin flips and thus line broadening.<sup>18</sup> The fact that the temperature de-

pendence of the ESR linewidth arising from the mobile holes was observed only in the FIT1 line component would thus indicate that the mobile holes are associated with the V(1)-V(2) plane but not with the V(3) site.

In summary, water intercalation in dodecylamine-intercalated vanadium oxide nanotubes obtained by a sol-gel method was markedly identified by means of x-ray diffraction and Fourier-transform infrared spectroscopy measurements. Our electron spin resonance study showed that the mobile holes in the vanadium oxide nanotubes have something to do with the V(1)-V(2) planes but not with the V(3) site lying between them and that intercalated water molecules give rise to an increase in the  $\text{V}^{4+}$  ion concentration and to changes in the magnetic interactions between the spins at distinct vanadium sites.

#### ACKNOWLEDGMENTS

This work was supported by the Korea Science and Engineering Foundation [User Program of Proton Engineering Frontier Project, M60504000021-05B0400-02110 (joint Korean-Israeli Research Grant No. 3-2217)] and by the Korea Research Foundation (Grant No. KRF-2004-005-C00060 and the Second Brain Korea 21 Project). This work was also supported by the Seoul Research and Business Development Program (Grant No. 10583). The measurements at the Korean Basic Science Institute (KBSI) are acknowledged.

\*Author to whom correspondence should be addressed; rscel@korea.ac.kr

<sup>1</sup>X. Chen, X. Sun, and Y. Li, *Inorg. Chem.* **41**, 4524 (2002); J. W. Jang, C. E. Lee, S. C. Lyu, T. J. Lee, and C. J. Lee, *Appl. Phys. Lett.* **84**, 2877 (2004).

<sup>2</sup>M. Niederberger, H.-J. Muhr, F. Krumeich, F. Bieri, D. Gunther, and R. Nesper, *Chem. Mater.* **12**, 1995 (2000); M. H. Park, J. W. Jang, C. E. Lee, and C. J. Lee, *Appl. Phys. Lett.* **86**, 023110 (2005).

<sup>3</sup>F. Krumeich, H.-J. Muhr, M. Niederberger, F. Bieri, B. Schnyder, and R. Nesper, *J. Am. Chem. Soc.* **121**, 8324 (1999); J. Park, E. Lee, K. W. Lee, and C. E. Lee, *Appl. Phys. Lett.* **89**, 183114 (2006).

<sup>4</sup>Y.-J. Liu, J. L. Schindler, D. C. DeGroot, C. R. Kannewurf, W. Hirpo, and M. G. Kanatzidis, *Chem. Mater.* **8**, 525 (1996).

<sup>5</sup>Z. F. Li and E. Ruckenstein, *Langmuir* **18**, 6956 (2002).

<sup>6</sup>L. Krusin-Elbaum, D. M. News, H. Zeng, V. Derycke, J. Z. Sun, and R. Sandstrom, *Nature (London)* **431**, 672 (2004).

<sup>7</sup>J. Cao, J. Choi, J. L. Musfeldt, S. Lutta, and M. S. Whittingham, *Chem. Mater.* **16**, 731 (2004).

<sup>8</sup>A. Doble, K. Ngala, S. Yang, P. Y. Zavalij, and M. S. Whittingham, *Chem. Mater.* **13**, 4382 (2001).

<sup>9</sup>X. Liu, C. Taschner, A. Leonhardt, M. H. Rummeli, T. Pichler, T. Gemming, B. Buchner, and M. Knupfer, *Phys. Rev. B* **72**, 115407 (2005).

<sup>10</sup>T. Chirayil, P. Y. Zavalij, and M. S. Whittingham, *Chem. Mater.* **10**, 2629 (1998).

<sup>11</sup>M. Demeter, M. Neumann, and W. Reichelt, *Surf. Sci.* **454-456**, 41 (2000).

<sup>12</sup>E. Vavilova, I. Hellmann, V. Kataev, C. Taschner, B. Buchner, and R. Klingeler, *Phys. Rev. B* **73**, 144417 (2006).

<sup>13</sup>W. Chen, L. Mai, J. Peng, Q. Xu, and Q. Zhu, *J. Solid State Chem.* **177**, 377 (2004).

<sup>14</sup>G. T. Chandrappa, N. S. Teunou, Cassaignon, C. Bauvais, and J. Livage, *Catal. Today* **78**, 85 (2003).

<sup>15</sup>X. Wu, Y. Tao, L. Dong, and J. Hong, *J. Mater. Chem.* **14**, 901 (2004).

<sup>16</sup>L. Yu and X. Zhang, *Mater. Chem. Phys.* **87**, 168 (2004).

<sup>17</sup>P. Barboux, D. Gouruer, and J. Livage, *Colloids Surf.* **11**, 119 (1984).

<sup>18</sup>V. Kataev, K.-Y. Choi, M. Gruninger, U. Ammerahl, B. Buchner, A. Freimuth, and A. Revcolevschi, *Phys. Rev. B* **64**, 104422 (2001).

<sup>19</sup>W. Chen, L. Q. Mai, J. F. Peng, Q. Xu, and Q. Y. Zhu, *J. Mater. Sci.* **39**, 2625 (2004).

<sup>20</sup>S.-H. Lee, H. M. Cheong, M. J. Seong, P. Liu, C. E. Tracy, A. Mascarenhas, J. R. Pitts, and S. K. Deb, *Solid State Ionics* **165**, 111 (2003).

<sup>21</sup>A. G. S. Filho, O. P. Ferreira, E. J. G. Santos, J. M. S. Filho, and O. L. Alves, *Nano Lett.* **4**, 2099 (2004).

<sup>22</sup>V. A. Ioff and I. B. Patrino, *Sov. Phys. Solid State* **10**, 639 (1968).

<sup>23</sup>J. L. Ragle, *J. Chem. Phys.* **38**, 2020 (1963).

<sup>24</sup>A. Kahn, J. Livage, and R. Collongues, *Phys. Status Solidi A* **26**, 175 (1974); K. W. Lee, E. M. Lee, H. Kweon, J. Park, and C. E. Lee, *J. Korean Phys. Soc.* **49**, 1625 (2006).

<sup>25</sup>M. J. Saeki, M. A. Aegerter, V. Sargentelli, and A. O. Florentino, *J. Sol-Gel Sci. Technol.* **25**, 83 (2002).